Local and Nonlocal Electron Dynamics of Au/Fe/MgO(001) Heterostructures Analyzed by Time-Resolved Two-Photon Photoemission Spectroscopy

Y. Beyazit,[1] J. Beckord,[1,*] P. Zhou,[1] J. P. Meyburg,[2] F. Kühne,[2] D. Diesing,[2] M. Ligges,[1,†] and U. Bovensiepen[1,‡]
[1]Faculty of Physics and Center for Nanointegration (CENIDE), University of Duisburg-Essen, Lotharstrasse 1, 47057 Duisburg, Germany
[2]Faculty of Chemistry, University of Duisburg-Essen, Universitätsstrasse 5, 45141 Essen, Germany

(Received 28 October 2019; revised 6 March 2020; accepted 7 July 2020; published 14 August 2020)

Employing femtosecond laser pulses in front and back side pumping of Au/Fe/MgO(001) combined with detection in two-photon photoelectron emission spectroscopy, we analyze local relaxation dynamics of excited electrons in buried Fe, injection into Au across the Fe-Au interface, and electron transport across the Au layer at 0.6 to 2.0 eV above the Fermi energy. By analysis as a function of Au film thickness we obtain the electron lifetimes of bulk Au and Fe and distinguish the relaxation in the heterostructure's constituents. We also show that the excited electrons propagate through Au in a superdiffusive regime and conclude further that electron injection across the epitaxial interface proceeds ballistically by electron wave packet propagation.

DOI: 10.1103/PhysRevLett.125.076803

Excited charge carriers relax in metals and semiconductors on femtosecond to picosecond timescales due to the large phase space for electron-electron (e-e) and electron-phonon scattering [1,2]. Microscopic insight into these processes was developed by combined efforts of static spectroscopy, spectroscopy in the time domain, and *ab initio* theory [3]. Early optical experiments used schemes in which the back side of the sample is pumped and the front side is probed and analyzed the propagation dynamics through the bulk of thin films [4]. Time- and angle-resolved two-photon photoelectron spectroscopy exploited the sensitivity to electron energy and momentum and was key to develop a comprehensive understanding of the microscopic nature of the engaged elementary processes which hot electrons experience [5–9]. In heterostrutures such an analysis is challenging but highly desired given the widespread application of these material systems. The surface sensitivity of photoelectron spectroscopy is a severe limitation for heterostructures and buried media which can be overcome by using hard x-ray photons in photoemission [10,11]. Also, photoelectrons with low kinetic energy are reported to probe the bulk [12] or buried interface electronic structure [13,14] in selected cases.

Hot electrons are characterized by their energy above the Fermi energy $E - E_F \gg k_B T$, where T is the equilibrium temperature, and their momentum $\mathbf{k}$. For a component $k_\perp$ directed from the surface into bulk, transport effects occur. So far, local dynamics at the surface and nonlocal contributions due to, e.g., transport were distinguished indirectly by analyzing relaxation at surfaces [15–19]. Particular systems allowed a microscopic description of electron propagation through a molecular layer [20] and resonant tunneling across a dielectric film [13].

Electronic transport properties are essential in condensed matter. Besides transport in Bloch bands at E_F, problems like incoherent hopping in molecular wires [21] and two-dimensional materials [22,23], superdiffusive spin currents [24], and attosecond phenomena at surfaces [25] are important. The relevance of spin-dependent charge carrier transport in femtosecond magnetization dynamics has spurred the use of back side pumping in optical pump-probe experiments [26–28], which provide energy and momentum integrated information. Also, detection in microscopes provides insight into carrier propagation [29] and plasmon dynamics [30]. Back side pump–front side probe photoelectron spectroscopy might have considerable impact, since it promises energy- and momentum-dependent information [29].

In this Letter we report such a back side pump–front side probe photoemission experiment for the model system Au/Fe/MgO(001). While for thin films the electronic relaxation agrees for front and back side pumping, we identify electron transport for thicker Au films upon back side pumping. We are aware that the dynamics has a spin-dependent contribution [26]. The experiment performed here is spin integrating and we focus on the charge dynamics. By analyzing the relaxation time dependence on the Au film thickness d_{Au} we distinguish the electron dynamics in the Au and Fe constituents.

Figure 1, top, depicts the experimental configuration. Femtosecond laser pulses are generated by a commercial regenerative Ti:sapphire amplifier (Coherent RegA 9040) combined with a noncollinear optical parametric amplifier (NOPA, Clark-MXR) operating at 250 kHz repetition rate. We use pairs of 2 and 4 eV pulses each of 50 fs pulse duration as pump and probe pulses, respectively. Pump pulses are sent to the Au/Fe/MgO(001) sample kept at

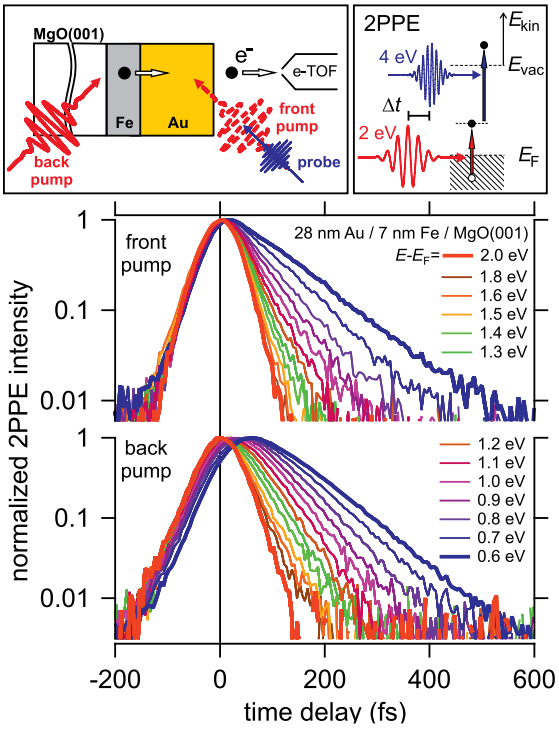

FIG. 1. Top: Schematic experimental configuration for front or back side pumping depicting the photoelectron analysis and the two-color 2PPE process for absorption of one 2 and 4 eV photon each. Bottom: Time-dependent 2PPE intensity on a logarithmic scale for front (top) and back side pumping (bottom) at indicated energies above the Fermi level.

room temperature with ±45° angle of incidence, see Fig. 1, and reach at first the Au surface in the case of front side pumping or are transmitted through MgO(001) and excite electrons of Fe in back side pumping. The incident pump fluence was 50 μJ/cm^2. Probe pulses are in both configurations sent to the Au surface close to 45° and probe electrons in intermediate, excited states (i) at the surface in case of front side pumping or (ii) propagating through Au for back side pumping. The time-delayed probe pulse photoemits electrons from the excited state by absorption of one 4 eV photon, see Fig. 1, top right, and generates the two-color two-photon photoemission (2PPE) signal discussed here. Photoelectrons are analyzed by a time-of-flight (e-TOF) analyzer [31] and collected within ±11° off the surface normal; see Fig. 1. For a discussion of one- and two-color 2PPE, see Supplemental Material [32]. The Au/Fe/MgO(001) system was chosen due to its epitaxial structure [33] and inert surface. Samples are grown by molecular beam epitaxy, stored under Ar atmosphere, transferred in ambient conditions to the photoemission chamber, and cleaned by heating to 80 °C. Crystalline order and layer thickness were analyzed on a twin sample by cross-sectional transmission electron microscopy, magnetometry, profilometry, and atomic force microscopy; see Refs. [28,32,34].

Figure 1 shows the time-dependent 2PPE intensity for back and front side pumping at selected energies $E - E_F$ for 28 nm Au/7 nm Fe/MgO(001). Time zero is defined by the fastest signal given by the intensity maximum of electrons at the maximum kinetic energy; see $E - E_F =$ 2.0 eV in Fig. 1 [35]. The upper panel depicts front side pump 2PPE data. The lower panel shows results for back side pumping which exhibit a shift in time delay of the intensity built up and maximum increasing with decreasing $E - E_F$. This effect is assigned to delayed arrival of excited electrons at the Au-vacuum interface. Both datasets exhibit slower intensity relaxation for lower $E - E_F$ due to the respective increase in hot electron lifetime [2].

Figure 2 compares back side pump 2PPE for different Fe thickness d_{Fe} [Fig. 2(a)] and for different d_{Au} [Fig. 2(b)]. While in the case of larger d_{Au} transport effects are identified through a time shift in arrival at the Au surface, increasing of d_{Fe} results essentially in a loss of intensity. Note that such loss of intensity is also observed with increasing d_{Au}, see Supplemental Material [32], because only electrons which reach the Au-vacuum interface are detected. These observations support the following concept. The Fe layer acts as the optically excited electron emitter and the Au layer serves as the acceptor hosting electron propagation as depicted by the scheme in Fig. 1.

Time-dependent 2PPE intensities are fitted by a single exponential decay $\propto \exp\frac{t-t_0}{\tau}$ convolved with the cross-correlation (XC) of the laser pulses as determined by 2PPE at maximum kinetic energy. Examples of such fits are plotted as insets in Figs. 3(a) and 3(b). This fitting determines energy-dependent, inelastic relaxation times $\tau(E)$ and time offsets $t_0(E)$, at which the relaxation starts. Figure 3 shows $\tau(E)$ and $t_0(E)$ obtained for $d_{Au} = 28$ nm [Fig. 3(a)] and 5 nm [Fig. 3(b)] at $d_{Fe} = 7$ nm. We find a decrease in τ with increasing energy and—if compared at identical energies—τ is larger for the thicker than for the thinner Au layer. Front and back side pumping lead to small differences in $\tau(E)$ near 1.2 eV for $d_{Au} = 28$ nm. Such differences were not obtained for $d_{Au} = 5$ nm, neither in τ nor in t_0. For sufficiently thin films transport effects become negligible [17] and $d_{Au} = 5$ nm provides a

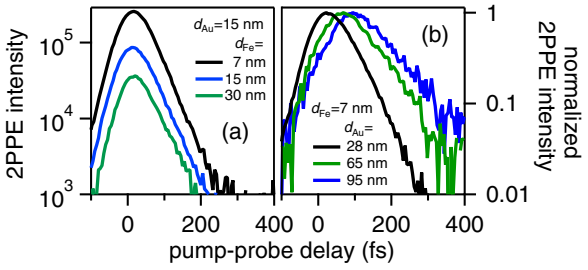

FIG. 2. Time-dependent 2PPE intensity upon back side pumping at $E - E_F = 1.0$ eV shown in (a) for different d_{Fe} and constant d_{Au} and vice versa in (b). In the latter case the 2PPE intensity is normalized to the intensity maximum.

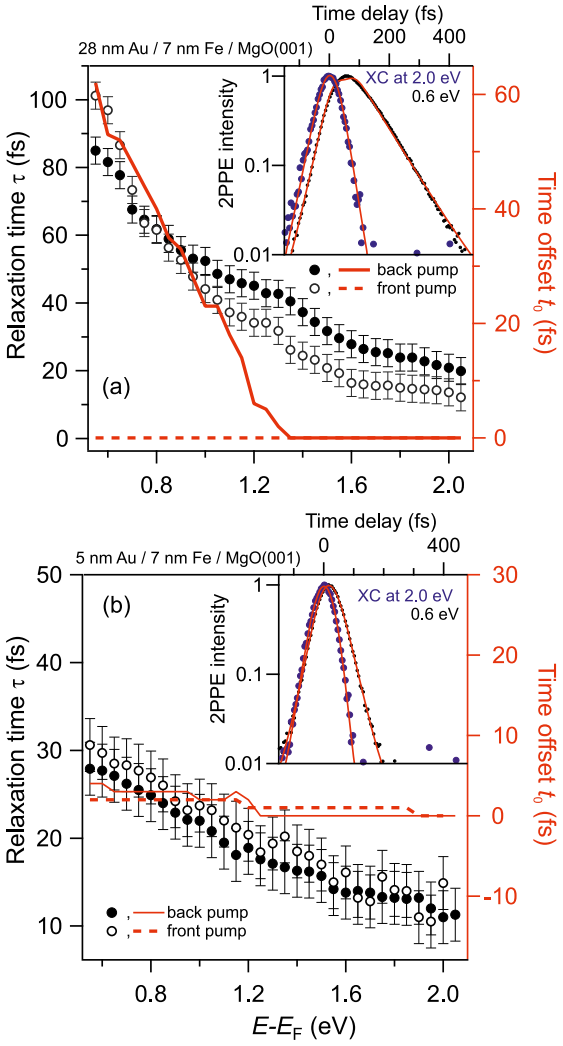

FIG. 3. Left axis: Relaxation times τ of hot electrons at energies $E - E_F$ for 28 nm (a) and 5 nm (b) thick Au films on 7 nm Fe on a MgO(001) substrate. Right axis: Time offset t_0; see text. Both quantities are determined by fitting and are given for front and back side pumping as indicated. Error bars for t_0 are ± 6 fs at 0.7 eV and decrease to ± 3 fs at 2.0 eV.

reasonable reference value in this regard. For $d_{\mathrm{Au}} = 28$ nm we identify for back side pumping variations in $t_0(E)$ up to 60 fs while $t_0(E)$ does not vary for front side pumping. The observed $t_0 > 0$ for back side pumping is a nonlocal effect and quantifies the time required for transport of electrons excited in Fe, injected into Au across the Fe-Au interface, and propagation through Au toward the Au-vacuum interface, where they are probed in 2PPE. Following bulk optical constants [36], 95% of the absorbed pump pulse intensity excites the 7 nm Fe layer and the 2PPE signal detected for 28 nm Au/7 nm Fe/MgO(001) is dominated by electrons propagating through Au. This assignment is supported by the increase in t_0 and τ for the larger d_{Au} compared to the thinner one; see Fig. 3. Since relaxation times of hot electrons in metals at few eV energy above E_F are determined by inelastic e-e scattering [2], the similar trend of increasing t_0 and τ with decreasing energy indicates that t_0 is determined by inelastic e-e scattering as well. On this basis the electron transport through Au is concluded to proceed in a superdiffusive regime, which occurs before hot electrons have thermalized by subsequent e-e scattering events [37]. As discussed in Supplemental Material [32], reaching the limit of diffusion would require many scattering processes, which we exclude due to the observation $t_0(E_0) < \tau(E_0)$, which implies individual events. Ballistic propagation, on the other hand, would occur for absent relaxation, which disagrees with the observed temporal broadening in time-dependent 2PPE intensities while the electrons propagate through Au; see Fig. 2(b). Given the weak variation of the electron group velocity with respect to the Fermi velocity in Au [38], ballistic propagation is also incompatible with the increase in t_0 observed with decreasing energy. Scattering might increase the covered distance to the surface and a determination of the electron's propagation velocity $v = d_{\mathrm{Au}}/t_0$ which results for $d_{\mathrm{Au}} = 28$ nm at $E - E_F = 1.0$ eV in $v = 1.3$ nm/fs—a value close to v_F in Au—has to be treated with care. We note that we cannot exclude ballistic propagation of electrons $E - E_F \geq 1.3$ eV where we find $t_0 = 0$ fs, which is set by the time zero determination.

We investigate $d_{\mathrm{Au}} = 5$–95 nm and identify a thickness-dependent $\tau = \tau(d_{\mathrm{Au}})$, see Figs. 2 and 3. The obtained τ are for thinner films smaller than in bulk Au [2]. Figure 4, top, shows $\tau(d_{\mathrm{Au}})^{-1}$ for different energy. To understand this thickness dependence we consider a continuum approach to scattering in the heterostructure, which assumes that the individual thicknesses d_{Au}, d_{Fe} and the extension of the interface $d_{\mathrm{Au-Fe}}$ are comparable with the respective scattering lengths $\lambda_i \approx \tau_i v_{F,i}$, which are $\approx$50 nm in Au and $\approx$2 nm in Fe [28,39]. The integral scattering probability of electrons propagating in the interface normal direction z increases linearly with d_{Au}, d_{Fe}, and $d_{\mathrm{Au-Fe}}$:

$$\int_0^{d_{\mathrm{Fe}}+d_{\mathrm{Au-Fe}}+d_{\mathrm{Au}}} \frac{dz}{\tau(z)} = \frac{d_{\mathrm{Fe}}}{\tau_{\mathrm{Fe}}} + \frac{d_{\mathrm{Au-Fe}}}{\tau_{\mathrm{Au-Fe}}} + \frac{d_{\mathrm{Au}}}{\tau_{\mathrm{Au}}}. \quad (1)$$

In our 2PPE back side pump–front side probe experiment, the variation of d_{Au} allows separation of two independent processes, see Supplemental Material [32], described by

$$\frac{1}{\tau(d_{\mathrm{Au}})} = \frac{1}{\tau_1} + \frac{1}{\tau_2} = A + \frac{B}{d_{\mathrm{Au}}}. \quad (2)$$

Figure 4, top, depicts fits following Eq. (2) with A and B being the intercept with the ordinate and slope as a function of $1/d_{\mathrm{Au}}$, respectively. Note that both A and B/d have the dimension of a rate. Our analysis determines relaxation times τ_1 and τ_2 which are plotted in Fig. 4, bottom, in comparison with literature values for hot electron lifetimes in bulk Au and Fe τ_{Au}, τ_{Fe}, respectively, taken from

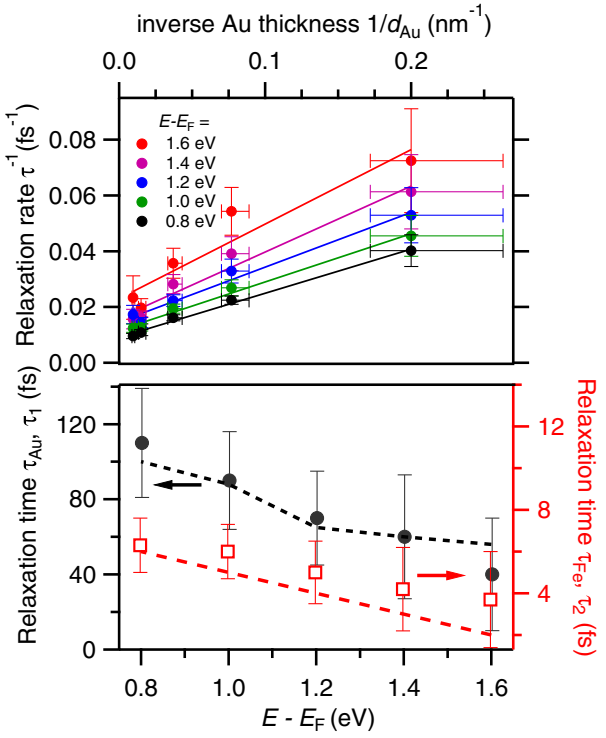

FIG. 4. Top: Relaxation rates τ^{-1} as a function of d_{Au}^{-1} for different electron energies above E_F. Lines represent linear fits. Slopes and intercepts determine the two relaxation rates discussed in the text. Bottom panel: The determined relaxation times τ_1 (•) and τ_2 (□) as a function of $E - E_F$ in comparison with literature data for hot electron lifetimes τ_{Au} and τ_{Fe} from Ref. [2] shown by dashed lines.

Ref. [2]. Given the agreement of our data with these values, we conclude to have distinguished the electron dynamics in the two constituents and thereby demonstrate sensitivity to the buried Fe film.

The observation of τ_{Au} is straightforward to understand. A hot electron injected into Au at the Fe-Au interface propagates through the Au film and reaches the surface where it is photoemitted. During the propagation it experiences inelastic e-e scattering with rates of bulk Au and transfers energy to a secondary electron. We detect this scattering by the time-dependent reduction of 2PPE intensity at the energy of interest at which the electrons were injected into Au. We did not take secondary electrons into account because we restricted the energy scale to rather high values $E - E_F$, where primary electrons dominate [17]. Secondary electrons start to contribute at half the primary energy [2], which is $E - E_F < 1$ eV for the highest energy electrons at 2 eV studied here. For sufficiently thick Au films, the second term in Eq. (2) vanishes and scattering in Au dominates.

Understanding the determination of τ_{Fe} in buried Fe requires consideration of all processes that may contribute to B in Eq. (2). Following Eq. (1) we take scattering in Fe and at the Au-Fe interface into account. Since we find within the experimental uncertainty $\tau_2 = \tau_{Fe}$, we conclude that the scattering at the interface does not contribute. In the investigated epitaxial heterostructure electron injection across the interface can be assumed to proceed by coherent propagation of a wave packet in Bloch states which conserves energy and momentum across the interface [18,34]. Therefore, the injection process across the Au-Fe interface is ballistic and violates our above assumption $d_{Au-Fe} \approx \lambda_{Au-Fe}$, which might be reason for not detecting it.

In addition, the reported approach provides opportunities to analyze scattering at buried interfaces originating from (i) electronic interface states and (ii) scattering at non-epitaxial interfaces for heterostructures in general. While (i) might be investigated in an analysis following Eq. (2) through the appearance of anomalies in the energy-dependent relaxation times and lead to deviations from the smooth variation reported in Fig. 4, the impact of (ii) can be determined by changing the thickness of both constituents as introduced in Eq. (1). As detailed in Ref. [32], this would lead to an additional term in Eq. (2) representing scattering at the interface.

In conclusion, we demonstrate a time-domain analysis of electron dynamics in epitaxial Au/Fe/MgO(001) heterostructures with a total thickness of 12–102 nm. We distinguish the energy-dependent scattering rates in Fe and Au using optical pumping of Fe and detection at the Au surface by two-photon photoemission. We also identify the electron propagation to proceed in a superdiffusive regime. This separation of electron dynamics in the individual heterostructure constituents showcases the impact our approach might have on future work. A spectroscopy which accesses buried interfaces or media and provides energy-dependent information on electron dynamics is rarely available and may provide highly desired insight into heterostructures in general. We expect that this approach will bridge conventional transport measurements and time-domain spectroscopy. Implementing angle- and spin-resolved detection of photoelectrons will provide momentum- and spin-dependent information and a more comprehensive understanding of electron dynamics in complex materials. We expect further that this approach to electron transport dynamics will be applied to semiconducting or insulating material systems due to its sensitivity to excited electronic states.

We acknowledge A. Eschenlohr for fruitful discussions and S. Salamon for experimental support. This work was funded by the Deutsche Forschungsgemeinschaft (DFG, German Research Foundation) Project No. 278162697—SFB 1242.

Note added in proof.—We mention a recent report of spin- and time-resolved photoemission of spin currents, see [40].

*Present address: University of Zurich, 8057 Zurich, Switzerland.

[†]Present address: Fraunhofer IMS, 47057 Duisburg, Germany.
[‡]uwe.bovensiepen@uni-due.de

[1] J. Shah, *Ultrafast Spectroscopy of Semiconductors and Semiconductor Nanostructures*, 2nd ed. (Springer, Berlin, 1999).
[2] M. Bauer, A. Marienfeld, and M. Aeschlimann, Hot electron lifetimes in metals probed by time-resolved two-photon photoemission, Prog. Surf. Sci. **90**, 319 (2015).
[3] P. M. Echenique, R. Berndt, E. Chulkov, T. Fauster, A. Goldmann, and U. Höfer, Decay of electronic excitations at metal surfaces, Surf. Sci. Rep. **52**, 219 (2004).
[4] S. D. Brorson, J. G. Fujimoto, and E. P. Ippen, Femtosecond Electronic Heat-Transport Dynamics in Thin Gold Films, Phys. Rev. Lett. **59**, 1962 (1987).
[5] N.-H. Ge, C. M. Wong, R. L. Lingle, J. D. McNeill, K. J. Gaffney, and C. B. Harris, Femtosecond dynamics of electron localization at interfaces, Science **279**, 202 (1998).
[6] M. Weinelt, M. Kutschera, T. Fauster, and M. Rohlfing, Dynamics of Exciton Formation at the Si(100) c(4 × 2) Surface, Phys. Rev. Lett. **92**, 126801 (2004).
[7] J. Güdde, M. Rohleder, T. Meier, S. W. Koch, and U. Höfer, Time-resolved investigation of coherently controlled electric currents at a metal surface, Science **318**, 1287 (2007).
[8] *Dynamics at Solid State Surfaces and Interfaces*, edited by U. Bovensiepen, H. Petek, and M. Wolf (Wiley-VCH, Berlin, 2012), Vol. 1.
[9] X. Cui, C. Wang, A. Argondizzo, S. Garrett-Roe, B. Gumhalter, and H. Petek, Transient excitons at metal surfaces, Nat. Phys. **10**, 505 (2014).
[10] J. C. Woicik, *Hard X-Ray Photoelectron Spectroscopy* (Springer, Heidelberg, 2016).
[11] L.-P. Oloff, M. Oura, K. Rossnagel, A. Chainani, M. Matsunami, R. Eguchi, T. Kiss, Y. Nakatani, T. Yamaguchi, J. Miyawaki *et al.*, Time-resolved HAXPES at SACLA: Probe and pump pulse-induced space-charge effects, New J. Phys. **16**, 123045 (2014).
[12] T. Kiss, F. Kanetaka, T. Yokoya, T. Shimojima, K. Kanai, S. Shin, Y. Onuki, T. Togashi, C. Zhang, C. T. Chen *et al.*, Photoemission Spectroscopic Evidence of Gap Anisotropy in an f-Electron Superconductor, Phys. Rev. Lett. **94**, 057001 (2005).
[13] M. Rohleder, W. Berthold, J. Güdde, and U. Höfer, Time-Resolved Two-Photon Photoemission of Buried Interface States in Ar/Cu(100), Phys. Rev. Lett. **94**, 017401 (2005).
[14] L. Rettig, P. S. Kirchmann, and U. Bovensiepen, Ultrafast dynamics of occupied quantum well states in Pb/Si(111), New J. Phys. **14**, 023047 (2012).
[15] M. Aeschlimann, M. Bauer, S. Pawlik, R. Knorren, G. Bouzerar, and K. H. Bennemann, Transport and dynamics of optically excited electrons in metals, Appl. Phys. A **71**, 485 (2000).
[16] M. Lisowski, P. A. Loukakos, U. Bovensiepen, J. Stähler, C. Gahl, and M. Wolf, Ultra-fast dynamics of electron thermalization, cooling and transport effects in Ru(001), Appl. Phys. A **78**, 165 (2004).
[17] M. Lisowski, P. A. Loukakos, U. Bovensiepen, and M. Wolf, Femtosecond dynamics and transport of optically excited electrons in epitaxial Cu films on Si(111) − 7 × 7, Appl. Phys. A **79**, 739 (2004).
[18] J. P. Gauyacq, A. G. Borisov, and M. Bauer, Excited states in the alkali/noble metal surface systems: A model system for the study of charge transfer dynamics at surfaces, Prog. Surf. Sci. **82**, 244 (2007).
[19] P. S. Kirchmann, L. Rettig, X. Zubizarreta, V. M. Silkin, E. V. Chulkov, and U. Bovensiepen, Quasiparticle lifetimes in metallic quantum-well nanostructures, Nat. Phys. **6**, 782 (2010).
[20] J. Stähler, M. Meyer, D. O. Kusmierek, U. Bovensiepen, and M. Wolf, Ultrafast electron transfer dynamics at NH_3/Cu (111) interfaces: determination of the transient tunneling barrier, J. Am. Chem. Soc. **130**, 8797 (2008).
[21] A. A. Kocherzhenko, S. Patwardhan, F. C. Grozema, H. L. Anderson, and L. D. A. Siebbeles, Mechanism of Charge Transport along Zinc Porphyrin-Based Molecular Wires, J. Am. Chem. Soc. **131**, 5522 (2009).
[22] A. S. Ngankeu, S. K. Mahatha, K. Guilloy, M. Bianchi, C. E. Sanders, K. Hanff, K. Rossnagel, J. A. Miwa, C. Breth Nielsen, M. Bremholm *et al.*, Quasi-one-dimensional metallic band dispersion in the commensurate charge density wave of $1T - TaS_2$, Phys. Rev. B **96**, 195147 (2017).
[23] S.-H. Lee, J. S. Goh, and D. Cho, Origin of the Insulating Phase and First-Order Metal-Insulator Transition in $1T - TaS_2$, Phys. Rev. Lett. **122**, 106404 (2019).
[24] M. Battiato, K. Carva, and P. M. Oppeneer, Superdiffusive Spin Transport as a Mechanism of Ultrafast Demagnetization, Phys. Rev. Lett. **105**, 027203 (2010).
[25] Z. Tao, C. Chen, T. Szilvási, M. Keller, M. Mavrikakis, H. Kapteyn, and M. Murnane, Direct time-domain observation of attosecond final-state lifetimes in photoemission from solids, Science **353**, 62 (2016).
[26] A. Melnikov, I. Razdolski, T. O. Wehling, E. T. Papaioannou, V. Roddatis, P. Fumagalli, O. Aktsipetrov, A. I. Lichtenstein, and U. Bovensiepen, Ultrafast Transport of Laser-Excited Spin-Polarized Carriers in Au/Fe/MgO(001), Phys. Rev. Lett. **107**, 076601 (2011).
[27] N. Bergeard, M. Hehn, S. Mangin, G. Lengaigne, F. Montaigne, M. L. M. Lalieu, B. Koopmans, and G. Malinowski, Hot-Electron-Induced Ultrafast Demagnetization in Co/Pt Multilayers, Phys. Rev. Lett. **117**, 147203 (2016).
[28] I. Razdolski, A. Alekhin, N. Ilin, J. P. Meyburg, V. Roddatis, D. Diesing, U. Bovensiepen, and A. Melnikov, Nanoscale interface confinement of ultrafast spin transfer torque driving non-uniform spin dynamics, Nat. Commun. **8**, 15007 (2017).
[29] J. Sung, C. Schnedermann, L. Ni, A. Sadhanala, R. Y. S. Chen, C. Cho, L. Priest, J. M. Lim, H.-K. Kimand, B. Monserrat *et al.*, Long-range ballistic propagation of carriers in methylammonium lead iodide perovskite thin films, Nat. Phys. **16**, 171 (2020).
[30] A. Klick, M. Großmann, M. Beewen, P. Bittorf, J. Fiutowski, T. Leißner, H.-G. Rubahn, C. Reinhardt, H.-J. Elmers, and M. Bauer, Femtosecond time-resolved photoemission electron microscopy operated at sample illumination from the rear side, Rev. Sci. Instrum. **90**, 053704 (2019).

[31] P. S. Kirchmann, L. Rettig, D. Nandi, U. Lipowski, M. Wolf, and U. Bovensiepen, A time-of-flight spectrometer for angle-resolved detection of low energy electrons in two dimensions, Appl. Phys. A **91**, 211 (2008).

[32] See Supplemental Material at http://link.aps.org/supplemental/10.1103/PhysRevLett.125.076803 for detailed information on the samples, the experimental method, and the continuum model for electron transport.

[33] M. Rickart, B. F. P. Roos, T. Mewes, J. Jorzick, S. O. Demokritov, and B. Hillebrands, Morphology of epitaxial metallic layers on MgO substrates: Influence of submonolayer carbon contamination, Surf. Sci. **495**, 68 (2001).

[34] A. Alekhin, I. Razdolski, N. Ilin, J. P. Meyburg, D. Diesing, V. Roddatis, I. Rungger, M. Stamenova, S. Sanvito, U. Bovensiepen *et al.*, Femtosecond Spin Current Pulses Generated by the Nonthermal Spin-Dependent Seebeck Effect and Interacting with Ferromagnets in Spin Valves, Phys. Rev. Lett. **119**, 017202 (2017).

[35] In case of ballistic electron propagation through Au the back side optical excitation would occur at negative time delays given by the Fermi velocity, which is for Au $v_F \approx 1.4$ nm/fs [4,36], multiplied with d_{Au}.

[36] J. H. Weaver, C. Krafka, D. W. Lynch, and E. E. Koch, *Optical Properties of Metals*, Physics Data (Fachinformationszentrum, Karlsruhe, 1981), Vols. 18–1,18–2.

[37] M. Battiato, K. Carva, and P. M. Oppeneer, Theory of laser-induced ultrafast superdiffusive spin transport in layered heterostructures, Phys. Rev. B **86**, 024404 (2012).

[38] D. M. Nenno, B. Rethfeld, and H. C. Schneider, Particle-in-cell simulation of ultrafast hot-carrier transport in Fe/Au heterostructures, Phys. Rev. B **98**, 224416 (2018).

[39] V. P. Zhukov, E. V. Chulkov, and P. M. Echenique, Lifetimes and inelastic mean free path of low-energy excited electrons in Fe, Ni, Pt, and Au: Ab initio $GW + T$ calculations, Phys. Rev. B **73**, 125105 (2006).

[40] K. Bühlmann, G. Saerens, A. Vaterlaus, and Y. Acremann, Detection of femtosecond spin injection into a thin gold layer by time and spin resolved photoemission, Sci. Rep. **10**, 12632 (2020).